Bonding in metal disilicides $CaSi_2$ through $NiSi_2$: Experiment and theory

J. H. Weaver and A. Franciosi
Department of Chemical Engineering and Materials Science, University of Minnesota, Minneapolis, Minnesota 55455

V. L. Moruzzi
IBM Thomas J. Watson Research Center, Yorktown Heights, New York 10598

(Received 20 October 1983)

Synchrotron radiation photoemission experiments with the disilicides of Ti, V, Nb, Cr, Fe, Co, and Ni are combined with self-consistent augmented-spherical-wave calculations of the density of states for metal silicides from Ca-Si to Cu-Si. These results demonstrate the importance of silicon p—metal d bond formation extending to ~ 6 eV below E_F for all transition metals. Experiment and theory are combined to show the movement of the nonbonding d states from above E_F for Ca-Si to well below E_F for Cu-Si. At the same time, the antibonding Si p and Si s states are shown to be relatively insensitive to the particular metal atom in the silicide series.

INTRODUCTION

The transition-metal silicides have properties which make them scientifically interesting and, at the same time, extremely important for the microelectronics industry. Many of them are chemically stable and resistant to corrosion or degradation, some form at relatively low temperature and have high electrical conductance,[1,2] others show promise as interface diffusion barriers,[3] and an increasing number of silicides are finding application in very-large-scale integrated (VLSI) circuit technology. Substantial efforts are now underway to understand the electronic properties of silicides and silicide-silicon junctions.[4–7]

We have undertaken a series of experimental and theoretical studies to delineate the role of the Si s, the Si p, and the metal d states in bonding and band-structure properties of a variety of transition-metal silicides.[8–12] This is part of a broader study which seeks insight not only about the bulk silicides but also about the electronic and structural evolution of metal-silicon interfaces.[12–15] In this paper, we present angle-integrated synchrotron radiation photoemission results for the bulk disilicides $TiSi_2$, VSi_2, $NbSi_2$, $CrSi_2$, $FeSi_2$, $CoSi_2$, and $NiSi_2$. Self-consistent augmented-spherical-wave (ASW) calculations performed for model metal-silicon compounds in the high-symmetry CuAu and Cu_3Au structures allow us to model the density of states for disilicides for comparison with experiment. These results reveal the dependence of the band structure on d-band occupancy and they demonstrate the common characteristics of transition-metal silicides, including the nonbonding d states near E_F, the p-d hybridized states extending to ~ 6 eV below E_F, and the Si s states 10—14 eV below E_F. For $CoSi_2$ and $NiSi_2$, which exhibit the CaF_2 structure, results from several different calculations are compared with experiment.

It should be pointed out that some of the silicides discussed herein have been examined by other authors, and Gelatt, Williams, and Moruzzi[8] have reported detailed theoretical studies of bonding between 4d transition metals and the non-transition-metal elements Li through F. Many of the observations regarding the p-d bond are therefore common to this excellent previous work. The point of this paper is to present a systematic study of bonding valid for all of the metal silicides, including the alkaline-earth and near-noble-metal silicides.

EXPERIMENTAL AND THEORETICAL TECHNIQUES

Buttons of the disilicides of Ti, V, Nb, Cr, Fe, Co, and Ni were initially prepared by arc melting high-purity constituents in a nonconsumable arc furnace on a water-cooled copper hearth. The success and ease of this process varied from silicide to silicide but the resulting 50-g samples were generally solid and homogeneous and further processing was limited to annealing to promote grain growth.[16] In particular, this arc-melting procedure was very satisfactory for $TiSi_2$, VSi_2, $NbSi_2$, $CrSi_2$, and $CoSi_2$ because they formed congruently from the melt. The disilicide $NiSi_2$ forms peritectically and the reaction was completed by annealing at 940 °C for six days. $FeSi_2$ is reported to form congruently at 1220 °C, but this alloy was also heat treated for homogenization at 940 °C for 13 days. For $CrSi_2$, the initial arc melting was followed by float-zone melting to ensure uniform composition.

Samples of these silicides were prepared for synchrotron radiation photoemission studies by fracturing precut posts *in situ* in the spectrometer at operating pressures of $\sim 5\times 10^{-11}$ Torr. Radiation from the Tantalus 240-MeV electron storage ring was used for studies in the range $10 \leq h\nu \leq 140$ eV (Grasshopper or toroidal grating monochromators). Photoelectron energy analysis was done with a commercial double-pass electron energy analyzer. The overall resolution of the experimental features varied from ~ 0.35 eV, depending on the photon energy. The results presented here are representative of stoichiometric-metal disilicides because the samples were fractured *in situ*. Effects due to segregation at the surface of silicides thermally grown on silicon or surface enrichment of one component due to preferential sputtering are thus avoided. At

the same time, such effects are interesting because of their importance in interface phenomena, and comparison with our spectra is informative.[11,12]

The experimental energy distribution curves (EDC's) shown in this paper have been scaled to give an approximately constant height for the dominant feature. At the same time, absolute $h\nu$ dependences of the photoionization cross sections were determined through normalization of the emission intensity to the photon flux.

The phase diagram of silicides generally show a variety of stable phases. In the experimental phase of this study, we emphasize the disilicides, because the disilicide is the most common interface reaction product and because we sought systematics in bonding within a particular stoichiometry range. The structural complexity of silicides has, no doubt, hindered the development of detailed theoretical pictures of their electronic structures.[17] Few calculations have been attempted which are, at the same time, descriptive of the correct stoichiometry and crystal structure and are also self-consistent. The calculations presented here are based on the cubic CuAu and Cu_3Au structures. They show systematics in bonding as a function of stoichiometry and, more important for this paper, changes in the Si-derived and metal-derived states as the metal itself is varied across the 3*d* transition series. Site and angular momentum decomposed state densities derived from model calculations of this kind have been shown to adequately describe the general trends of chemical bonding between transition metals and non-transition metals. For example, the behavior of the *p-d* states as a function of stoichiometry and the estimates of charge transfer as derived from such calculations and from calculations using realistic silicide structures were found to be in remarkable agreement for Ni and Pd silicides.[18,19]

The energy-band calculations were based on the augmented-spherical-wave (ASW) procedure for the solution of the one-electron equations.[20] Exchange and correlation effects were treated in the local-density approximation. Self-consistency was pursued until the calculated electronic charges were unchanged to within 0.001 electrons within the Wigner-Seitz sphere. The calculations were parameter-free, the only *a priori* inputs being atomic number and crystal structure, and they correspond to theoretical equilibrium since the atomic spacing was systematically varied until the total energy was minimized.

GENERAL TRENDS IN SILICIDE BONDING

In Fig. 1, we show calculated densities of states (DOS's) for the 3*d* transition-metal monosilicides based on the

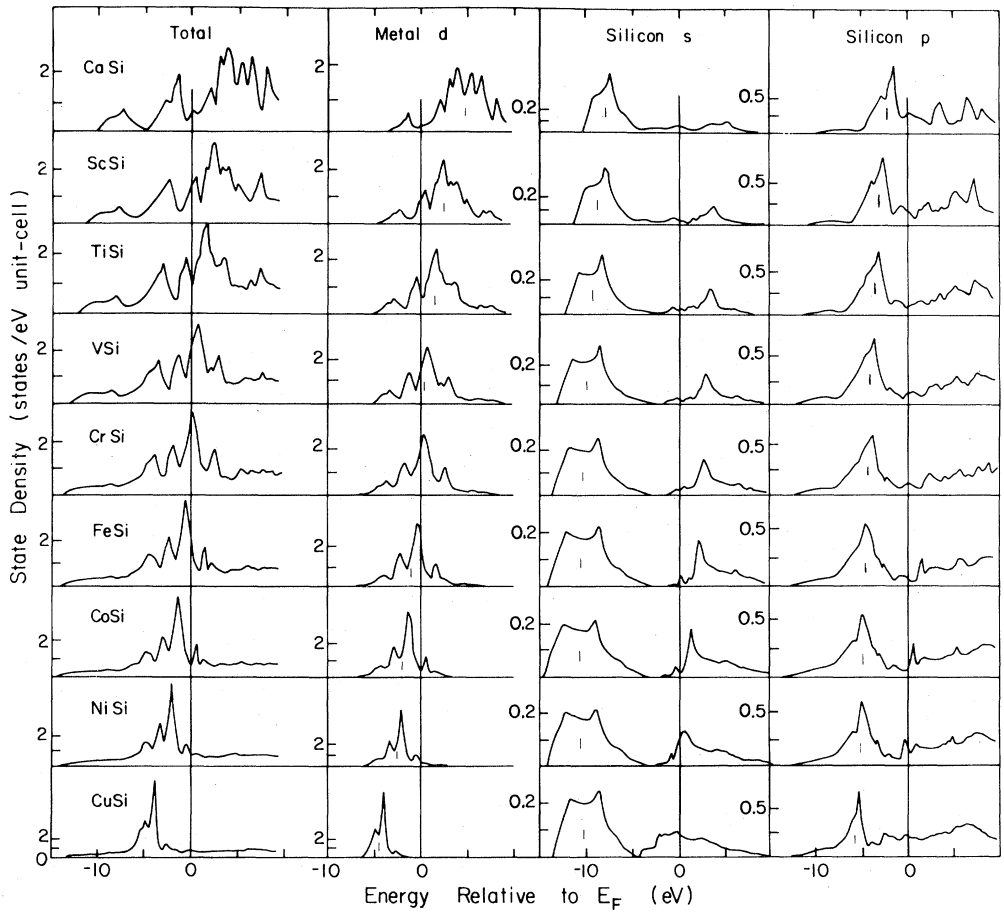

FIG. 1. Calculated total and partial state densities for monosilicides of Ca (top) through Cu (bottom) in the CuAu crystal structure. The scales are given alongside each curve. Tic marks guide the eye in observing systematics with increasing atomic number, including the movement of the *d* bands through the Si *p* bands.

CuAu structure. In Fig. 2, we show analogous results for the trisilicides ($CuAu_3$ structure). The total DOS is shown on the left of each figure, the l-projected metal d character is shown next, and these are followed by the projected silicon s and p character.

The results of Figs. 1 and 2 show how the d bands dominate the DOS and move through E_F with increasing Z, as indicated by tic marks at the center of the bands. This motion is relatively slow when the d-band density of states is high at E_F (near the middle of the transition series) but is faster at the extremes (near Ca-Si or Cu-Si). The metal d-derived states vary substantially within the series, appearing first as a broad band of mostly empty states for Ca-Si and ending with the narrow, fully occupied d band for Cu-Si. It is important to note that these results always show d character well below E_F—even for Ca which has s^2d^0 electronic configuration in the atom. This d character results from the lowering in energy of metal-derived $3d$ states that hybridize with Si-derived $3p$ states. The resulting p-d bonding combinations determine the stability of the silicide, while the corresponding antibonding combinations appear mostly above E_F.

The Si p—derived states are clustered into two energy regions straddling the Fermi level, with the occupied or bonding region being better defined than the empty states. As the atomic number of the metal atom is increased from Ca-Si to Cu-Si, the center of the occupied cluster moves to greater binding energy but the empty feature stays relatively fixed ~ 5 eV above E_F. This is indicated by the tic marks in the figures and is best seen for the trisilicides. The movement of the bonding states follows the shift of the metal d states to greater binding energy with increasing Z and is connected with the hybridization of silicon p orbitals with metal $3d$ states. The corresponding p-d antibonding combination above E_F appears nearly invariant in energy in the silicide series.

The s-derived states, which extend to ~ 15 eV below E_F, overlap relatively little with the p states of Si or the metal d states. The dominant structure represents an admixture of dominantly Si s and a slight amount of metal s character. For the monosilicides, this s band moves from -8 eV for CaSi to -10 eV for CuSi (see tic marks). For the trisilicides, it is almost stationary at -10 eV, except for $CaSi_3$ and $ScSi_3$. The empty s states, on the other hand, become prominent only after Sc-Si or Ti-Si, and the resulting structure ultimately shifts to near E_F.

The movement of the d bands through the Si p manifold in the silicide series substantially alters the overall density of states but has relatively little impact on the nature of the silicon p-metal d bonds. The calculations indi-

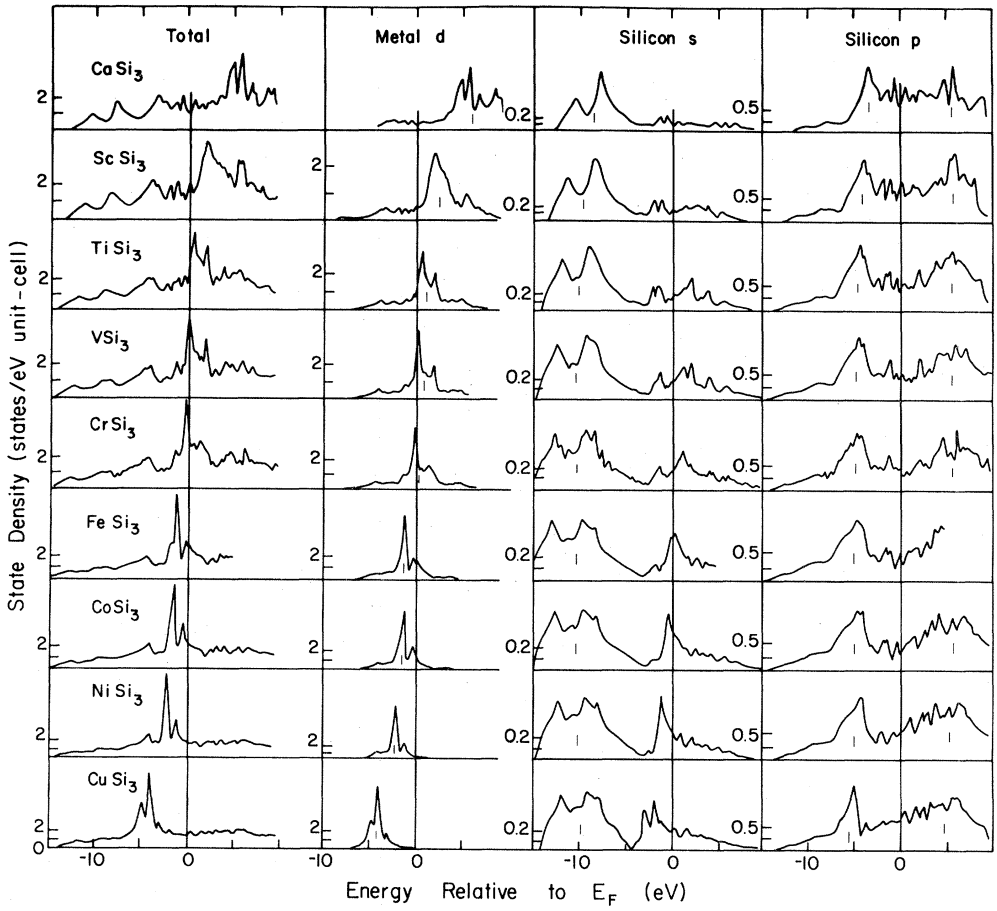

FIG. 2. Calculated total and partial state densities for the trisilicides of Ca (top) through Cu (bottom) analogous to those of Fig. 1 but with the $CuAu_3$ crystal structure.

cate that dominant silicon p—metal d coupling is present in all silicides, while the strength of such coupling varies with the relative position of the p and d states. In the trisilicide series, for example, p-d bonding combinations appear in the energy range 0.5—3.8 eV for $CaSi_3$ and involve virtually all the calculated d charge per metal atom. Moving along the 3d series, the shift and sharpening of the d bands yields p-d bonding states at 1.5—6 eV in $CrSi_3$ and 2.5—6.5 eV in $CoSi_3$, involving only about 50% of the calculated d charge per Cr atom in $CrSi_3$ and about 30% in $CoSi_3$. Correspondingly, the metal d states that are not directly coupled with Si p states form a cluster of nonbonding d states nearer E_F.

We emphasize that the systematics developed through Figs. 1 and 2 are based on isostructural calculations with hybridization of certain states allowed by group theory and forbidden to others. Calculations for different crystal structures will modify the details of the density of states. Nevertheless, we suggest that the bonding will always involve p-d hybridization and that these hybrid states will appear below the base of the nonhybridized states, in qualitative agreement with our results. This has been confirmed by recent calculations for VSi_2 (Ref. 21), $CrSi_2$, (Refs. 12 and 14), and $NiSi_2$ (Ref. 19) in their correct crystal structures.

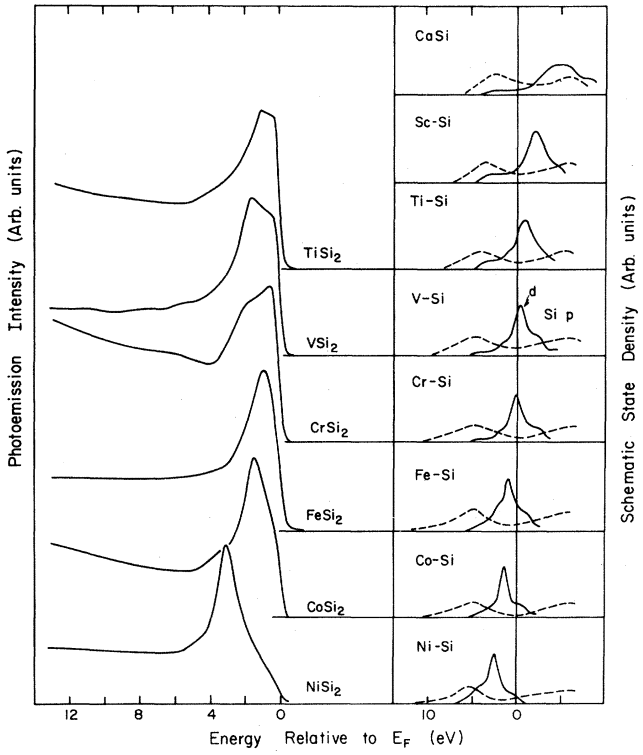

FIG. 3. Summary of experimental results (left) and interpolated state densities for the metal d (solid lines) and silicon p (dashed lines) states (right) for disilicides. Experiment verifies the existence of metal-silicon p-d bonding states extending to ~ 6 eV below E_F, as inferred from the calculations, and points to the common character of bonding in all transition-metal silicides. The dominant d emission near E_F corresponds to nonbonding states. Note that the results on the right are not scaled to true state densities.

COMPARISON OF EXPERIMENT AND THEORY

We see from the systematics of Figs. 1 and 2 that there are bonding d states below E_F for all these silicides. With increasing Z, the nonbonding d states sharpen, move through E_F, and, ultimately, even the antibonding states fall near E_F. To facilitate comparison of these predictions with our experimental results, we constructed qualitative DOS's for the disilicides based on results for the monosilicides and the trisilicides. To do this, we first broadened the monosilicides and trisilicides DOS features to retain only major features. These broadened DOS's were then compared and a *schematic* DOS was drawn which had the important points common to both but was, of course, insensitive to details. For example, the d character for CaSi was shown to extend ~ 4 eV below E_F with a broad cluster of states centered ~ 4.5 eV above E_F (width ~ 6 eV).

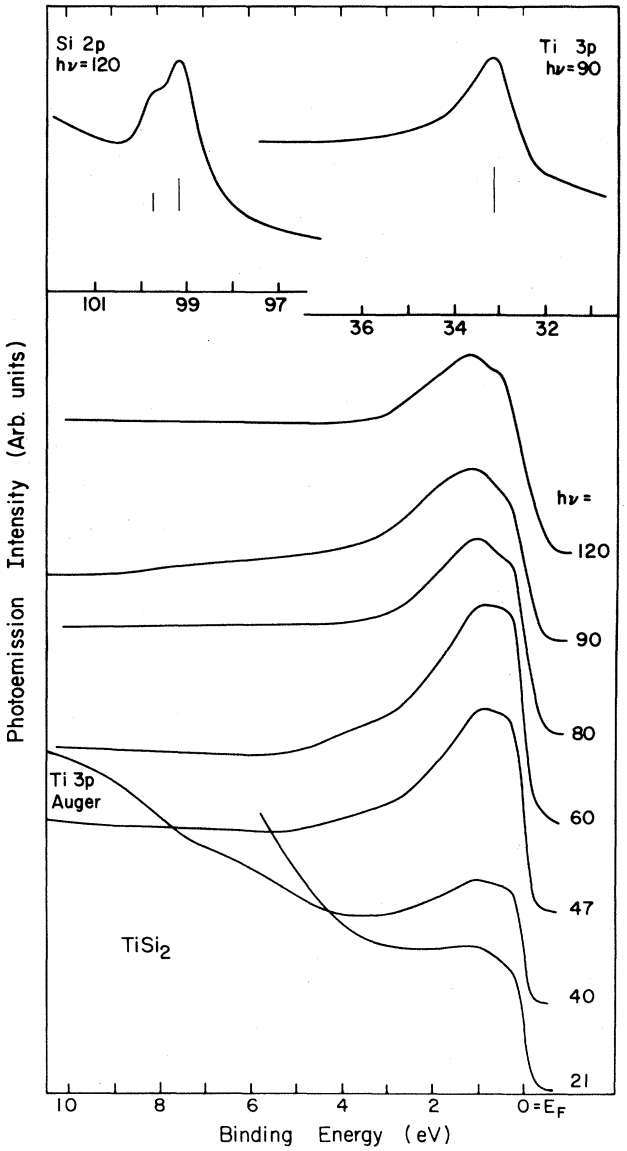

FIG. 4. Energy distribution curves (EDC's) for $TiSi_2$ for $21 \leq h\nu \leq 120$ eV. Emission from the Si 2p and Ti 3p cores is shown at the top.

For $CaSi_3$, the d character extended ~ 5 eV below E_F and the empty d states were centered ~ 6 eV above E_F (width 5.5—6 eV). Interpolation to $CaSi_2$ would indicate d character extending ~ 4.5 eV below E_F and empty states centered ~ 5 eV above E_F (width ~ 6 eV). Analogous procedures were used for the silicon p density of states. Hence, on the right of Fig. 3 we show the schematic DOS's for $CaSi_2$ and for the other systems under examination, using dashed curves for the Si p DOS's and solid curves for the metal d DOS's. Note that these DOS's are sketched with arbitrary units and that the d character dominates, as seen for the quantitative results of Figs. 1 and 2.

The interpolated p and d DOS's of Fig. 3 show that the d bands gather and disperse through E_F with increasing d occupancy, culminating in nearly filled d bands for $NiSi_2$. These interpolations predict clustered silicon p character ~ 5 eV below E_F. Hence, they preserve the most important aspect of the metal-silicon bond, namely, the p-d character well below E_F. They also establish the movement of the nonbonding d's through E_F with increasing Z. (These interpolated bands for $NiSi_2$ predict a DOS d peak ~ 2.5 eV below E_F, compared to ~ 2.8 eV from the calculations of Bisi and Calandra,[19] ~ 3.5 eV from Tersoff and Hamann,[22] or 3.3 eV from Bylander, Kleinman, Rednick, and Grise,[23] as will be seen in Fig. 10.)

In Figs. 4—10, we show EDC's for valence band and core emission for $TiSi_2$ (Fig. 4), VSi_2 (Fig. 5),[8] $NbSi_2$ (Fig. 6), $CrSi_2$ (Fig. 7),[12] $FeSi_2$ (Fig. 8), $CoSi_2$ (Fig. 9), and $NiSi_2$ (Fig. 10).[9] For visual clarity, the valence spectra have been offset and normalized to approximately the same height. The EDC's for the metal $3p$ ($4p$ for Nb) and Si $2p$ core levels are shown in the topmost or lowest sections of the figures. Since most valence-band features in Figs. 4—10 do not exhibit major dependence on $h\nu$ in the range

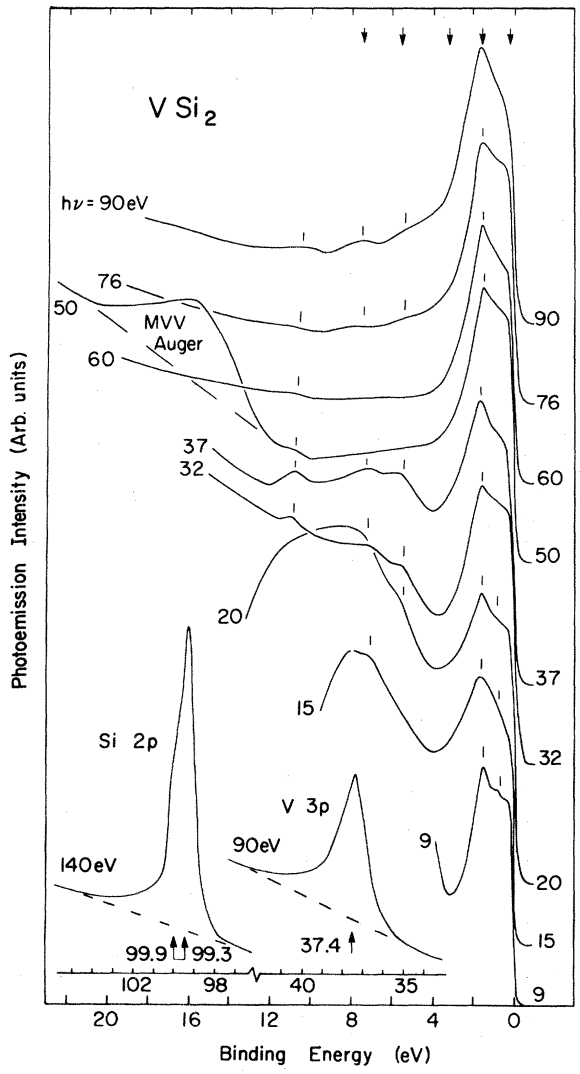

FIG. 5. EDC's for VSi_2 for $9 \leq h\nu \leq 90$ eV showing the $h\nu$ modulation of the initial states of nonbonding-d (near E_F), p-d hybrid (near 4 eV), p (near 6 eV), and s (near 10 eV) character.

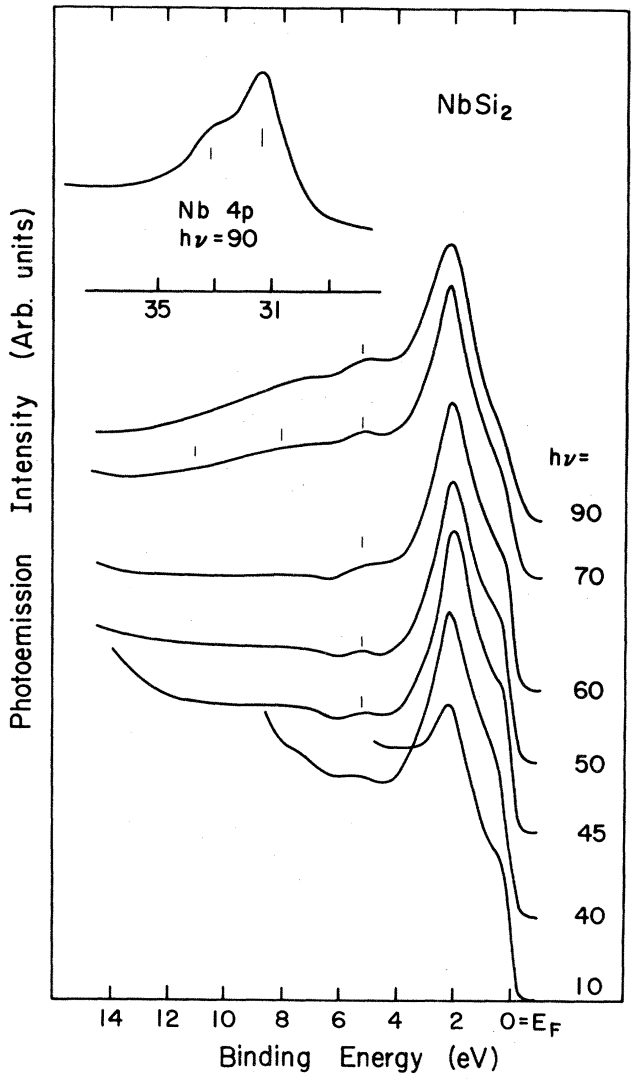

FIG. 6. EDC's for $NbSi_2$ in the photon energy range $10 \leq h\nu \leq 90$ eV for comparison to the $3d$ transition-metal disilicides. Emission from the Nb $4p$ cores is shown at the top. The valence-band spectra show s-, p-, p-d— and d-derived structures analogous to those for VSi_2.

$10 \leq h\nu \leq 120$ eV, we associated them with structure in the density of electronic states.

The spectra in Fig. 4 for $TiSi_2$ are dominated by intense emission within 3 eV of E_F (peak at 1—1.2 eV) and show a shoulder near 4 eV for $45 \leq h\nu \leq 65$ eV. At higher binding energies, emission above the secondary background is evident but it is without discernible structure. (Auger LVV emission appears near 9 eV in the 40-eV EDC.) For Ti-Si most of the d charge per atom is directly involved in the bonding with silicon and we associate the main spectral features to metal-derived $3d$ states. The schematic DOS in Fig. 3 suggests that the character of these valence states will become increasingly bonding for higher binding energies with a parallel increase of the Si-derived character of the valence states. The states that account for the DOS features 4 eV below E_F exhibit strong p-d hybrid character.

The valence-band spectra for VSi_2 in Fig. 5 show structure at 1.6, 5.5, 7.2, and 10.4 eV. The relative intensity of the EDC features is modulated by the different photoionization cross sections of initial states of s, p, or d character. On the basis of the results of Figs. 1 and 2 and of Ref. 21, we associate the feature at 1.6 eV with metal-derived $3d$ states, the feature at 5.5 eV with hybrid p-d orbitals, and the structures at 7.2 and 10.4 eV with relatively pure Si-derived p and s character, respectively. These identifications can be confirmed by a quantitative comparison of the cross section for the various initial states. Resonant photoemission at the $3p \rightarrow 3d$ excitation energy, in particular, has already been used for Pd_2Si (Ref. 10) to confirm the character of the different valence states. In the following section, we will apply this technique to VSi_2 as a test case for our systematic analysis of the disilicide valence states.

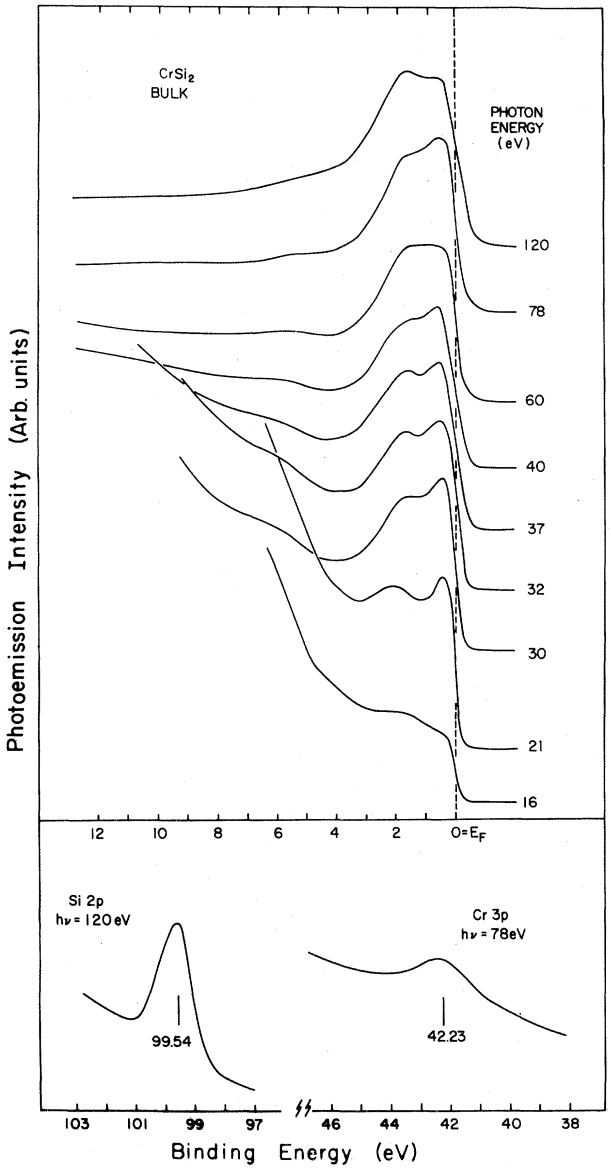

FIG. 7. EDC's for valence bands of $CrSi_2$ for $16 \leq h\nu \leq 120$ eV. Emission from the Si $2p$ and Cr $3p$ cores is shown in the lowest part of the figure (from Ref. 12).

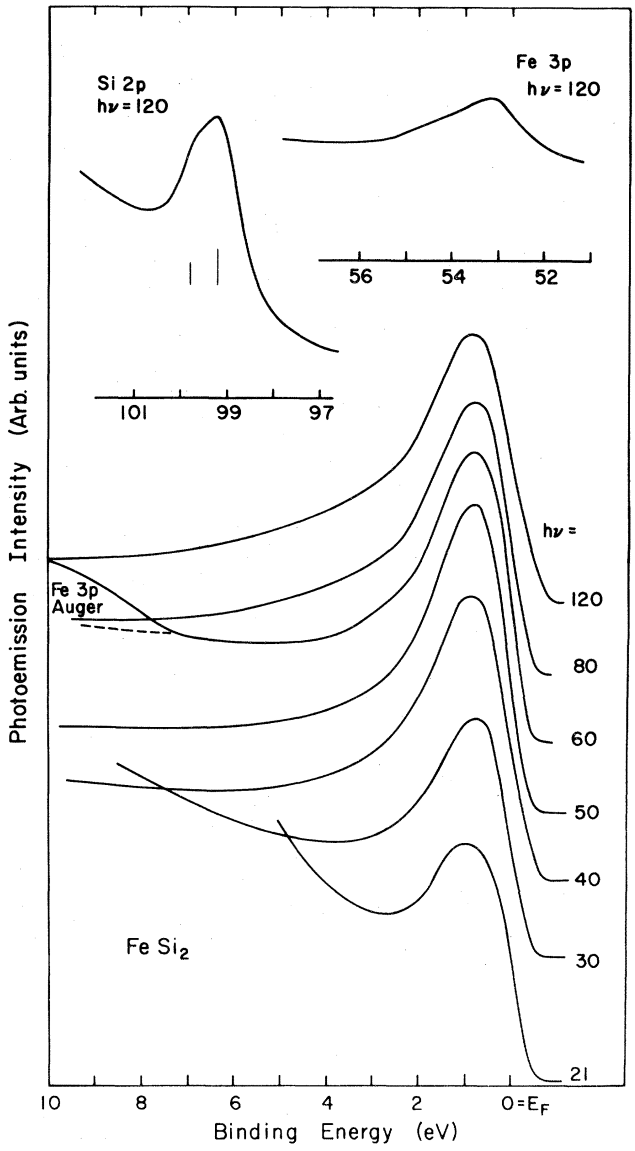

FIG. 8. EDC's for the valence bands of $FeSi_2$ for $21 \leq h\nu \leq 120$ eV. Emission from the Si $2p$ and Fe $3p$ cores is shown at the top.

In Fig. 6, we show EDC's for $NbSi_2$ for $10 \leq h\nu \leq 90$ eV. These, and results for $MoSi_2$,[8] provide a comparison for the $3d$ and $4d$ isoelectronic transition-metal disilicides. From them, we see that there are analogous spectral features for $NbSi_2$ and VSi_2 with slightly shifted binding energies (5.2, 8, and 11 eV for $NbSi_2$). The deepest can be related to the Si s-derived states and the two at 5.2 and 8 eV represent primarily p-derived features with substantial mixture of d character in the region of $\sim$4–6 eV. Further, these results show that the d-derived structure within $\sim$4 eV of E_F is wider for $NbSi_2$ than for VSi_2 because of the inherently wider d bands. This d-derived structure closely resembles that of $MoSi_2$ and the $5d$ transition-metal silicide $TaSi_2$.[8]

Valence-band and core data for $CrSi_2$ appear in Fig. 7 (from Ref. 12). The corresponding calculations in Figs. 1–3 indicate that the d bands for $CrSi_2$ are approximately half filled and that they draw away from E_F as they become nearly filled. Indeed, for $NiSi_2$ the d bands are predicted to be $\sim$3–6 eV below E_F. The effect of the d-band filling can be seen by examining the $CrSi_2$, $FeSi_2$, $CoSi_2$, and $NiSi_2$ silicide series (Figs. 3 and 7–10). The EDC's for $CrSi_2$ indicate strong emission near E_F (0.6 eV), structure near -2 eV, and a shoulder at -6 eV. The EDC's for $FeSi_2$ show less structure (peak at about 0.75 eV and broad, structureless emission extending to about -10 eV). EDC's for $CoSi_2$, on the other hand, show the dominant d-derived feature to have drawn away from E_F, as predicted by the interpolated DOS results of Fig. 3 (peak at 1.4–1.5 eV and shoulder at $\sim$3.8 eV below E_F). Results for $NiSi_2$, shown in Fig. 10 for $h\nu=40$ and 50 eV, are very similar to those for $CoSi_2$ except that the location of E_F is higher within the valence bands, the d bands are almost completely filled, and the separation of the nonbonding and bonding states is reduced.

These various results can be understood on the basis of the systematics of the schematic DOS of Fig. 3, taking into account the empirical observation that photoemission spectra for $10 \leq h\nu \leq 120$ eV emphasize nonbonding $3d$ states over the hybrid p-d orbitals. This can be seen, for example, by comparing the $NiSi_2$ calculations of Fig. 10 with experimental results or comparing our synchrotron radiation results[9] with XPS (x-ray photoelectron spectroscopy) results by Grunthaner, Madjukar, and Mayer for Ni_2Si.[7] In our EDC's the DOS structures 3–3.5 eV below E_F for $NiSi_2$ (2 eV for $CoSi_2$) dominate the spectra but the 5-eV feature (4 eV for $CoSi_2$) is much weaker than in the XPS results and in the calculations. Bearing this in mind, the experimental emission feature at 0.6 eV for $CrSi_2$ can be associated with nonbonding metal $3d$ states, while emission at 2.0 eV and below should come from bonding p-d orbitals. The shoulder at 6 eV corresponds to DOS features of substantial Si $-p$ character. Similarly, for $FeSi_2$, where a large fraction of the metal $3d$ charge is not coupled with Si-derived states, the main emission features within $\sim$2 eV of E_F reflect nonbonding metal d states, while the broad shoulder $\sim$5 eV below E_F exhibits mixed p-d character.

$CoSi_2$ is near the end of the $3d$ row where the nonbond-

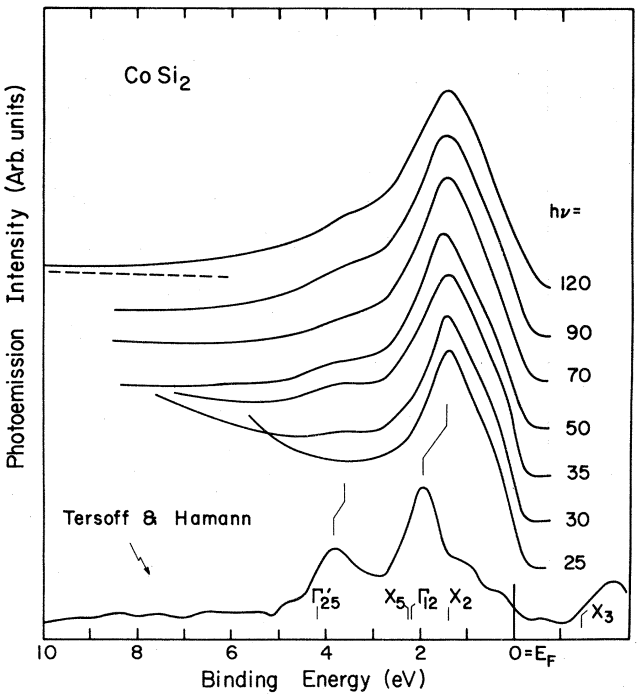

FIG. 9. EDC's for the valence bands of $CoSi_2$ in the photon energy range $25 \leq h\nu \leq 120$ eV compared to the total density of states calculated by Tersoff and Hamann (Ref. 22).

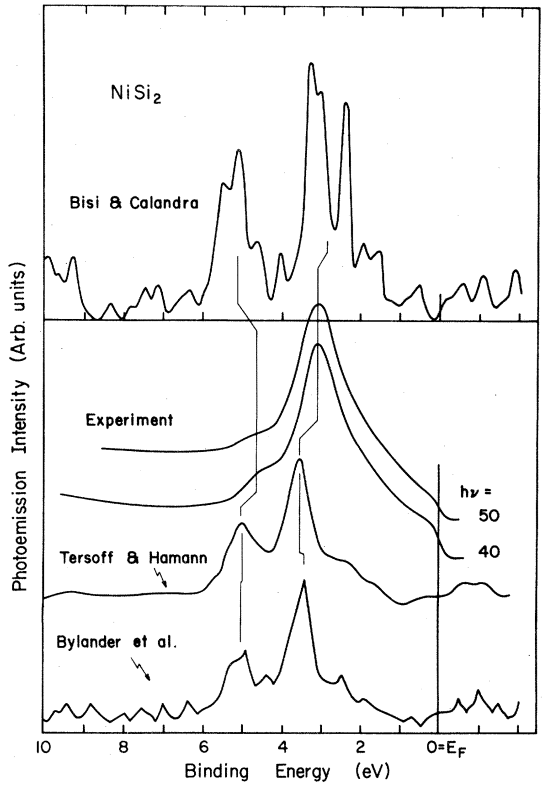

FIG. 10. EDC's for the valence bands of $NiSi_2$ for $h\nu=40$ and 50 eV (from Ref. 9). For comparison we show that total density of states calculated by Bisi and Calandra (Ref. 19) (top), Tersoff and Hamann (Ref. 22), and Bylander, Kleinman, Mednick, and Grise (Ref. 23) (bottom).

ing d states form a sharp, dominant emission feature at 1.45 eV and the bonding d states appear as a relatively weak structure at about 2-eV higher binding energy. In Fig. 9 we show the experimental results for $CoSi_2$ and compare them to the calculated density of states of Tersoff and Hamann.[22] Inspection shows quite good agreement but indicates that the calculations overestimate the binding energy of the experimental feature by 0.3—0.5 eV.

$NiSi_2$ is probably the most studied silicide both from the experimental and theoretical points of view. Angle-integrated and angle-resolved photoemission investigations of its electronic structure have recently been reported by ourselves,[9] Chang and Erskine, and Chabal, Hamann, Rowe, and Schlüter.[24] In Fig. 10 we summarize the angle-integrated results[9] and compare them to the densities of states calculated by Tersoff and Hamann,[22] Bisi and Calandra,[19] and Bylander, Kleinman, Mednick, and Grise.[23] As shown, there is good overall quantitative agreement with experiment and the different sets of calculations yield very similar densities of electronic states, although the details of the bonding vary from author to author (charge transfer and ionic contribution to the bond, electronic configuration at equilibrium for the metal and Si atoms).

RESONANT PHOTOEMISSION

Identification of the character of the valence states can be supported by quantitative analysis of the cross sections of the various initial states. To do this, we show in Fig. 5 a series of EDC's for VSi_2 and the results of analysis of the peak heights as a function of photon energy in Fig. 11. VSi_2 was chosen because several structures could be resolved in the valence bands, including features at 1.6 eV (d derived), 5.5 eV (p-d), 7.2 eV (p), and 10.4 eV (s derived). Emission from the Si-derived s and p states is low for $h\nu \simeq 50$—60 eV but then increases at higher energy. The d bands, on the other hand, are always prominent, but this is partially an artifact of normalization of the spectra of Fig. 5.

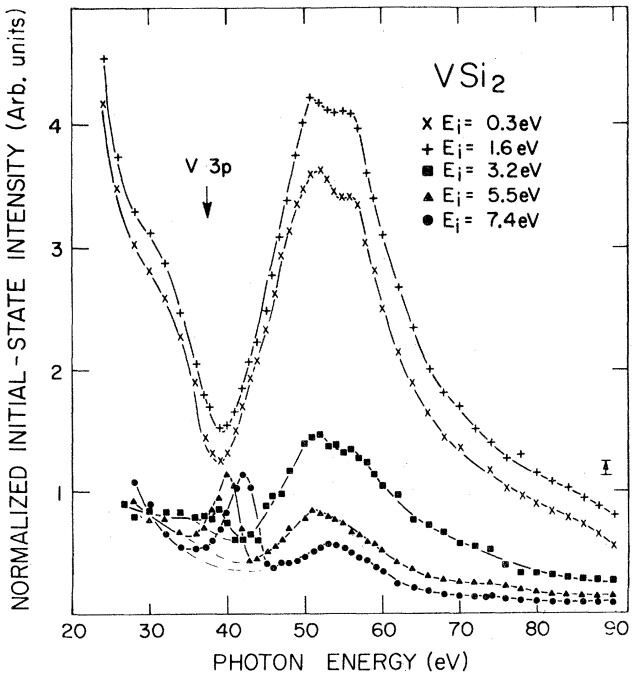

FIG. 11. Photoionization cross sections for VSi_2 corresponding to initial states marked by arrows in Fig. 5. As a result of $3p$-$3d$ resonance, the spectra show a threefold enhancement of the nonbonding d states. For the p-d hybrid states, the magnitude of the enhancement depends on the degree of hybridization and decreases for increasing Si p contribution.

Partial photoionization cross sections were determined from the spectra of Fig. 5 and others for $9 \leq h\nu \leq 90$ eV measured at increments of 1 or 2 eV. These are shown in Fig. 11 for initial states at 0.3, 1.6, 3.2, 5.5, and 7.4 eV (see arrows in Fig. 5). Clear enhancement of these states (and the entire band) for $h\nu \geq 38$ eV is associated with the excitation of the V $3p$ core ($E_B = 37.4$ eV). For $E_i = 0.3$ and 1.6 eV, the emission decreases for $20 \leq h\nu \leq 40$ eV but is then enhanced approximately threefold between ~ 38 and ~ 50 eV. For states in the p-d bonding region, the enhancement is weaker but the shape is approximately the same for $h\nu > 38$ eV. States with increased Si-derived character exhibit considerably less enhancement. (The structure that appears around $h\nu = 40$ eV is due to overlapping Auger emission.)

Resonant valence-band enhancement has been observed in other silicide systems[10] and is analogous to d-f enhancement studied in lanthanides and actinides.[25] This resonance reflects the quantum-mechanical equivalence of different paths leading from the ground state to the final state where an emitted electron is in the continuum. The two paths are direct valence-band emission $3p^6(4sd)^n + h\nu \rightarrow 3p^6(4sd)^{n-1} + e$ and a core-level-involving process $3p^6(4sd)^n + h\nu \rightarrow 3p^5(4sd)^{n+1} \rightarrow 3p^6(4sd)^{n-1} + e$. The strength of the enhancement is a measure of the overlap of the p-core hole and the d-valence state. Hence, as the d states become hybridized the overlap is reduced and the enhancement diminishes. The importance of this phenomenon to us here is that it can be used to highlight d emission in the photon energy range near the p-core-level excitation energy. The results for VSi_2 (as for Pd_2Si in Ref. 10) clearly show the different character of Si- and metal-derived states and they support the identification of the spectral feature as $3d$ derived, with mainly nonbonding character at E_F and increasing p-d hybrid character for increasing binding energy in the energy range 2—6 eV.

Cross-section analyses for $MoSi_2$ similar to those for VSi_2 show similar, but smaller, enhancement for $4p$-$4d$ interaction as for $3p$-$3d$. Analogous studies for ScH_2, YH_2, LaH_2, and ThH_2 (Ref. 26) indicate reduced enhancement for increasing principal quantum number n in np-nd resonance. This is due, in part, to the increasing delocalization of the d wave function.

CONCLUSIONS

In this paper we have given experimental and theoretical insight into bonding systematics for the metal disilicides over the full range of the $3d$ transition metals. The systematics indicate the following:

(1) The states which we see as dominant in synchrotron radiation photoemission are generally nonbonding $3d$ states since they overlap very little with Si-derived states. The results for the disilicides of Ti through Co all show important d character within 3 eV of E_F (lower for Ni). Hence, the electrical properties of silicides will be determined by d states.

(2) Silicon p—metal d mixing is important for all silicides and lowers metal d states to well below E_F. Our experimental observation of bonding mixtures of p-d states supports the model that p-d bonding states will generally account for the silicide stability. Detailed calculations of the future must consider the specifics of the p-d hybridization—this must vary with stoichiometry, crystal structure, and possibly nonequivalent sites (see, for example, the calculation of Switendick[27] for Fe_3Si).

(3) The detection of the Si s-derived states has, so far, been limited to the disilicides of V, Nb, Mo, Ta, and Ce. (Parks, Reihl, Martensson, and Steglich[28] have observed the onset of the Si s band near 12 eV for $CePd_2Si_2$ and $CeAu_2Si_2$.) For the other disilicides, we observe only an unstructured tailing off of valence-band emission near 10—12 eV. The invariance of this feature indicates that the Si s character is relatively unimportant in bonding.

We anticipate that these results can be generally interpolated to the monosilicides [e.g., MnSi and NiSi (Ref. 9)] and the metal-rich silicides [Fe_3Si, Ni_2Si (Ref. 9), Pd_2Si (Ref. 10)]. They will most likely find substantial validity for the germanides as well.

ACKNOWLEDGMENTS

It is a pleasure to acknowledge the staff of the Synchrotron Radiation Center of the University of Wisconsin, where the photoemission experiments were conducted, and the Materials Preparation Center of the Ames Laboratory, where the samples were prepared. Discussion with Dr. Tersoff, Dr. Kleinman, and Dr. Bisi are gratefully acknowledged. This work was supported by U. S. Army Research Office Contract No. ARO-DAAG-29-83-K-0061.

---

[1]K. N. Tu, in *Thin Films—Interdiffusion and Reactions,* edited by J. M. Poate, K. N. Tu, and J. W. Mayer (Wiley, New York, 1980).

[2]S. P. Murarka, J. Vac. Sci. Technol. 17, 775 (1980); G. Ottaviani, *ibid.* 18, 924 (1981).

[3]A. Franciosi, J. H. Weaver, and D. G. O'Neill, Phys. Rev. B 28, 4889 (1983).

[4]For an extensive review, see L. J. Brillson, Surf. Sci. Rep. 2, 123 (1982), and G. Margaritondo, Solid State Electron. 26, 499 (1983).

[5]L. Braicovich, I. Abbati, J. N. Miller, I. Lindau, S. Schwarz, P. R. Skeath, C. Y. Su, and W. E. Spicer, J. Vac. Sci. Technol. 17, 1005 (1980); I. Abbati, L. Braicovich, and B. De Michelis, Solid State Commun. 36, 145 (1980).

[6]J. L. Freeouf, G. W. Rubloff, P. S. Ho, and T. S. Kuan, Phys. Rev. Lett. 43, 1836 (1979); P. S. Ho, P. E. Schmid, and H. Foll, *ibid.* 46, 782 (1981).

[7]P. J. Grunthaner, F. J. Grunthaner, A. Madhukar, and J. W. Mayer, J. Vac. Sci. Technol. 19, 649 (1981); N. W. Cheung, P. J. Grunthaner, F. J. Grunthaner, J. W. Mayer, and B. M. Ullrich, *ibid.* 18, 917 (1981).

[8]J. H. Weaver, V. L. Moruzzi, and F. A. Schmidt, Phys. Rev. B 23, 2916 (1981) for VSi_2, $TaSi_2$, and $MoSi_2$. C. D. Gelatt, A. R. Williams, and V. L. Moruzzi [*ibid.* 27, 2005 (1983)] discussed bonding of $4d$ transition metals to the non-transition-metal elements Li through F and revealed how bonding changes when the s and p bands fall above, below, or near the d-band resonance.

[9]A. Franciosi, J. H. Weaver, and F. A. Schmidt, Phys. Rev. B 26, 546 (1982) for Ni_2Si, NiSi, and $NiSi_2$.

[10]A. Franciosi and J. H. Weaver, Phys. Rev. B 27, 3554 (1983) for Pd_2Si.

[11]A. Franciosi and J. H. Weaver [Physica (Utrecht) 117B-118B, 846 (1983), and Surf. Sci. 132, 324 (1983)] summarize results for a number of bulk and interface silicides.

[12]A. Franciosi, J. H. Weaver, D. G. O'Neill, F. A. Schmidt, O. Bisi, and C. Calandra [Phys. Rev. B 28, 7000 (1983)] present results for bulk and interface $CrSi_2$.

[13]A. Franciosi, D. J. Peterman, J. H. Weaver, and V. L. Moruzzi, Phys. Rev. B 25, 4981 (1982) for the Si(111)-Cr interface.

[14]A. Franciosi, J. H. Weaver, D. G. O'Neill, Y. Chabal, J. E. Rowe, J. M. Poate, O. Bisi, and C. Calandra, J. Vac. Sci. Technol. 21, 624 (1982) for the Si-Cr and Si-Ni interfaces.

[15]A. Franciosi, J. H. Weaver, P. Perfetti, A. D. Katnani, and G. Margaritondo, Solid State Commun. 47, 427 (1983) for the Si-Sm interface; A. Franciosi, J. H. Weaver, and D. T. Peterson (unpublished) for Si(111)-Ca.

[16]Visual examination of the microstructure showed $\lesssim 5\%$ intragranular second phase to be present for $FeSi_2$ and $CrSi_2$; this was confirmed by chemical analysis and x-ray analysis which indicated slightly silicon-rich average compositions.

[17]The crystal structure of these silicides include the $CrSi_2$ $C40$ structure ($CrSi_2$, VSi_2, $NbSi_2$), the hexagonal $TiSi_2$ $C54$ structure ($TiSi_2$), the hexagonal $MoSi_2$ $C11b$ structure ($MoSi_2$), the $FeSi_2$ structure ($FeSi_2$), and the CaF_2 $C1$ structure ($CoSi_2$, $NiSi_2$). These $MoSi_2$, $CrSi_2$, and $TiSi_2$ structures are all built up from close-packed layers and they differ only in their stacking sequences with stacking arrangement such that atoms have only two close neighbors in adjacent layers (10 nearest neighbors).

[18]P. S. Ho, G. W. Rubloff, J. E. Lewis, V. L. Moruzzi, and A. R. Williams, Phys. Rev. B 22, 4784 (1980).

[19]O. Bisi and C. Calandra, J. Phys. C 14, 5479 (1981).

[20]The ASW method as developed by A. R. Williams, J. Kubler, and C. D. Gelatt [Phys. Rev. B 19, 6094 (1979)] is the spherical wave analog of Slater's augmented-plane-wave (APW) method and is closely related to Andersen's linear combination of muffin-tin orbitals (LMTO) method; see, for example,

O. K. Andersen, *ibid.* 12, 3060 (1975).
[21]O. Bisi and L. W. Chiao, Phys. Rev. B 25, 4943 (1982).
[22]J. Tersoff and D. R. Hamann, Phys. Rev. B 28, 1168 (1983).
[23]D. M. Bylander, L. Kleinman, K. Mednick, and W. R. Grise, Phys. Rev. B 26, 6379 (1982).
[24]Yu-Jeng Chang and J. L. Erskine, Phys. Rev. B 26, 4766 (1982); Y. J. Chabal, D. R. Hamann, J. E. Rowe, and M. Schlüter, Phys. Rev. B 25, 7598 (1982).
[25]See, for example, D. J. Peterman, J. H. Weaver, M. Croft, and D. T. Peterson, Phys. Rev. B 27, 808 (1983), and detailed references therein on resonant photoemission.
[26]J. H. Weaver (unpublished).
[27]A. C. Switendick, Solid State Commun. 19, 511 (1976).
[28]R. D. Parks, B. Reihl, N. Martensson, and F. Steglich, Phys. Rev. B 27, 6052 (1983).